frontiers in Materials

ORIGINAL RESEARCH
published: 21 July 2020
doi: 10.3389/fmats.2020.00178

Preparation and Electrochemical Properties of Mesoporous $NiFe_2O_4$/N-Doped Carbon Nanocomposite as an Anode for Lithium Ion Battery

Jinli Zhang[1,2]* *and Zi-He Chen*[1,2]

[1] Department of Environmental Engineering, College of Harbour and Environmental Engineering, Jimei University, Xiamen, China, [2] Fujian Provincial Key Laboratory of Food Microbiology and Enzyme Engineering, Xiamen, China

The $NiFe_2O_4$/nitrogen doped carbon composite was synthesized via calcination of NiFe-MOF in a N_2 atmosphere. Nitrogen-doped carbon not only improves the conductivity of the carbon-based material, but also provides pathway, allowing Li^+ diffusion rapidly during the charge and discharge processes. The electrochemical data reveal that $NiFe_2O_4$/nitrogen-doped carbon nanocomposite delivers a capacity as high as 760 mAh·g^{-1} at 0.2 C after 50 cycles, and show good rate performance by remaining a capacity of 600 mAh·g^{-1} even at 1 C. The excellent electrochemical characteristics might be contributed to the $NiFe_2O_4$ ordered nanorod structure, well-marked porosity, and as well as the composition of nitrogen-doped carbon.

Keywords: $NiFe_2O_4$, anode, lithium-ion batteries, N-doped carbon, nanorod

OPEN ACCESS

Edited by:
Liang Huang,
Huazhong University of Science and Technology, China

Reviewed by:
Teng Zhai,
Nanjing University of Science and Technology, China
Xifeng Ding,
Nanjing University of Science and Technology, China

***Correspondence:**
Jinli Zhang
jlzhang@jmu.edu.cn

Specialty section:
This article was submitted to Energy Materials, a section of the journal Frontiers in Materials

Received: *06 April 2020*
Accepted: *13 May 2020*
Published: *21 July 2020*

Citation:
Zhang J and Chen Z-H (2020) Preparation and Electrochemical Properties of Mesoporous $NiFe_2O_4$/N-Doped Carbon Nanocomposite as an Anode for Lithium Ion Battery. Front. Mater. 7:178. doi: 10.3389/fmats.2020.00178

INTRODUCTION

Due to the concerns of environment protection, green energies have been intensively explored (Chen et al., 2018; Sun et al., 2018; Zhai et al., 2018). As one of the most popular energy storage devices, lithium ion batteries (LIBs) have been widely utilized in the portable electronic equipment from wireless communications to mobile computing due to their several advantages such as high energy density, low self-discharge, low maintenance, and longevity. Transition metal oxides (TMOs) have attracted much attention as the anodes for LIBs because of the merits such as low cost, environment-friendly, natural abundance, and high theoretical capacity compared with the commercially used graphitic material (Wu et al., 2015; Lian et al., 2016). In addition, the inherent high oxidation state characteristics of the 3D TMOs could transfer more than one electron per formula unit during the charge/discharge process as the full reduction of the transition metal atoms from their ionic to the metallic state, thus it is expected that higher current density would be obtained for TMOs LIBs.

Currently, more attention has been paid to bi-metallic oxides (Hong et al., 2020), specially spinel Fe-based binary metal oxides, e.g., $NiFe_2O_4$ (Yang H. et al., 2018), $ZnFe_2O_4$ (Wang et al., 2017a; Joshi et al., 2019), and $CoFe_2O_4$ (Xiong et al., 2014), and $CuFe_2O_4$ (Xing et al., 2013) for the reason that they could partially reduce the metal oxidation states and consequently re-oxidize to provide large reversible capacities. Moreover, it is possible to exist a confinement effect between the metal elements compared with the single-metal oxides (Bai et al., 2014; Wang et al., 2014). Compared with the Fe_2O_3, porous $NiFe_2O_4$ nanostructures would deliver higher capacities and exhibit a longer

cycling ability (Wang et al., 2016), which gains a theoretical capacity of 915 mAh g^{-1} (Luo et al., 2017). However, $NiFe_2O_4$ has a main weakness due to the large volume change during lithiation/de-lithiation process which results in rapid capacity loss and poor cycling life (Xiao et al., 2017). In this case, nanobox-, nanosphere-, and nanofiber-$NiFe_2O_4$ composited with carbon materials have been studied (Luo et al., 2015; Gao et al., 2017).

Many methods have been applied in the synthesis of bi-metal oxides, designing porous oxides with uniform and controllable nanostructures is an effective approach to further enhance their electrochemical properties (Wu et al., 2018; Yang S. et al., 2018), because the mesoporous nanostructure could effectively release the volume change during alloying/de-alloying with Li ions. Metal-organic frameworks (MOFs) are novel hybrid materials formed based on self-assembling metal ions with organic linkers. They usually own large specific surface areas and high porosity, which can be easily transformed into two-dimensional (2D) or three-dimensional (3D) porous metal oxides after calcination in air. In present work, taking bi-metallic NiFe-MOFs as the sacrificial template to fabricate porous $NiFe_2O_4$ nanostructure, which helps to maintain the porous 3D nanostructure of metal oxide and thus enhances the surface area to accommodate the volume change during cycling and as well as shortens the Li ions transport path, resulting in improvement of capacity retentions and rate performance (Maiti et al., 2018; Wang et al., 2018; Yang H. et al., 2018).

EXPERIMENTAL SECTION

Synthesis of NiFe-MOF Precursor

In general, 0.54 g $FeCl_3{\cdot}6H_2O$, 0.145 g $Ni(NO_3)_2{\cdot}6H_2O$, and 0.45 g 2-aminoterephthalic acid were dissolved in 27 ml N,N-dimethylformamide (DMF) under magnetic stirring. After 10 min, the solid powders were completely resolved, the solution became deep red. Then 3 mL 0.4 M NaOH was added into the solution, after 10 min stirring, the mixture solution was transferred into a 50 mL-size autoclave for another 12 h reaction at 100 °C. After that, the resulted suspension was centrifugated and washed with alcohol and DMF for three times, the obtained gel was then dried at 50°C for overnight to gain the NiFe-MOF precursor. **Figure S1** shows that FTIR spectrum of the as received NiFe-MOFs. The 3,350 and 3,450 cm^{-1} bands are according to the symmetric and asymmetric stretching vibrations of amino-group, and the IR peak at 1,660 cm^{-1} is assigned to the vibration of C = O band. These results indicate that the target compound has been successfully synthesized.

Preparation of Mesoporous $NiFe_2O_4$/Nitrogen-Doped Carbon Nanocomposite

The thermal gravimetric analysis (TGA) curve of the as prepared NiFe-MOF is shown in **Figure S2**. The loss of the adsorbed water displays from 50 to 100°C, and then the weight almost keeps constant until 330°C. About 45% mass loss appears from 333 to 480°C, which is attributed to the decomposition of organic framework (Zhou et al., 2014). When the temperature is further increased up to 500°C, the carbon component in the composite will be oxidized into CO_2 and finally leave metal oxides. Based on the TGA data, the as-received NiFe-MOF was loaded in an Al_2O_3 crucible placed in a quart tube furnace. After the NiFe-MOF was calcinated at 500°C for 2 h in N_2 atmosphere, the solid $NiFe_2O_4$/nitrogen-doped carbon ($NiFe_2O_4$/N-C) nanocomposite was therefore produced.

Characterization of the Materials

X-ray diffraction (XRD) were measured from 5°∼80° with a speed of 10°/min based on an X'pert PRO instrument using Cu Kα radiation (λ = 0.15418 nm). Scanning electron microscopy (SEM) images were obtained from Hitachi S-4,800. The special surface area was calculated using the Brunauer-Emmett-Teller (BET) method according to the adsorption data in the partial pressure (P/P_O) range 0.10–1.0. The total pore volume was determined from the amount of nitrogen adsorbed at P/P_O = 0.99. FTIR, X-ray photoelectron spectroscopy (XPS) detected with PHI 5,000 VBIII using Al kα monochromatic source.

Electrochemical Measurements

Electrochemical performances of the nanocomposite were measured on CR2016 coin-type cells assembled in an Ar-filled glove box. The working electrode was mixed $NiFe_2O_4$/N-C powders with Super P and LA binder at a weight ratio of 7:2:1. The mixture slurry was uniformly coated on a Cu foil and then dried at 100°C in vacuum for 24 h to remove the water. The counter electrode was simply used metallic lithium foil, the separator was Celgard 2,325 porous film, and the electrolyte was 1.0 M $LiPF_6$ solution dissolved in a mixed solvent of ethylene carbonate and diethyl carbonate (1:1 by volume). The cell capacity and life cycling tests were carried out with Newware BT-5 cell tester (Newware, Shenzhen) at room temperature with potential range from 0.005 to 3.0 V (vs. Li/Li^+). 1 C is equal to 1,000 mA g^{-1} in this work.

RESULTS AND DISCUSSION

Figure 1A displays SEM images of the as prepared NiFe-MOF. Homogeneous nanorod-like MOF structure is observed with length of 500 nm and width of 100 nm. After calcination at 500°C in N_2 atmosphere, because the NiFe-MOF is decomposed, SEM image of the resultant metal oxides and carbon matrix is thus indicated in **Figure 1B**. One may see that even after decomposition of the organic framework into carbon-based material, the nanostructure still largely maintains MOF original one, except for the slightly shortening in the length and shrinkage in the width. This result implies that the target composite nanostructure could be designed from its parent MOFs matrix.

Figure 2 shows XRD pattern of the NiFe-MOF derived composite. There is a weak and broad band existing between 20∼30°, which corresponds to carbon matrix similar to the previous study (Shao et al., 2017). Moreover, the XRD pattern reveals a set of reflections which could be indexed to the well-known spinel structure of ferrite with the space group of Fd-3m. The peaks at 2θ = 18.35°, 30.16°, 35.49°, 37.14°, 43.16°, 53.50°, 57.05°, and 62.65° could be accurately assigned to the

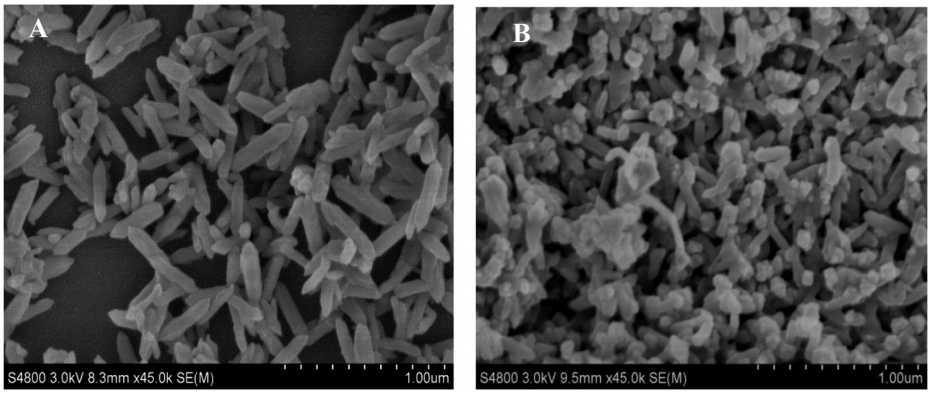

FIGURE 1 | The SEM images of **(A)** NiFe-MOF precursor and **(B)** NiFe$_2$O$_4$/N-doped carbon nanocomposite.

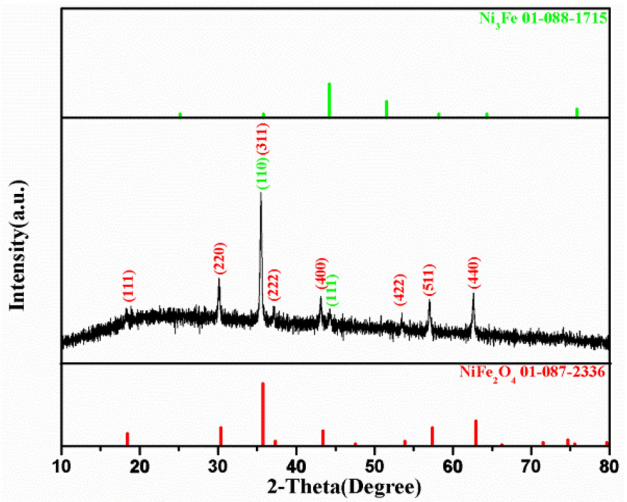

FIGURE 2 | The XRD pattern of NiFe$_2$O$_4$/N-C (middle), and JCPDS of Ni$_3$Fe (up) and NiFe$_2$O$_4$ (bottom).

diffractions of NiFe$_2$O$_4$ (111), (220), (311), (222), (400), (422), (511), and (440) phases, respectively, according to JCPDS 01-087-2336. The strong intensity and narrow peak width imply the good crystallinity of NiFe$_2$O$_4$ nanostructure. The spinel NiFe$_2$O$_4$ owns an anti-spinel crystalline structure, in which Ni^{2+} and half of Fe^{3+} cations locate at the octahedral positions, while the other half Fe^{3+} ions occupy the tetrahedral sites (Liu X. et al., 2017). It is interesting to find that besides the diffractions for NiFe$_2$O$_4$, a week peak exists at $2\theta = 44.31°$, which is resigned to Ni$_3$Fe based on JCPDS 01-088-1715. The formation of Ni$_3$Fe could be attributed to the further reaction of NiFe$_2$O$_4$ with the carbon matrix at 500°C in N_2 ambience as indicated in **Figure S2**. The presence of the metallic phase may enhance the electronic conductivity of the composite.

The porous characteristic of the prepared NiFe$_2$O$_4$/N-C composite was detected using the N_2 adsorption-desorption isotherm at 77 K. As shown in **Figure 3A**, there is an adsorption saturation platform and a hysteresis loop. According to the classification of the international union of pure and applied chemistry (IUPAC), the N_2 adsorption-desorption isotherm should belongs to type IV, which is the main characteristics of mesoporous materials. According to the BET method, the surface area of NiFe$_2$O$_4$/N-C composite is calculated to be 146.2 m^2/g. The corresponding pore-size distribution was then computed by Barrett-Joyner-Halenda (BJH) method from the isotherm depicts as indicated in **Figure 3B.** The pore size distribution is centered at 3.2 nm with a long tail until 15 nm. This identifies that the pore-size distribution is really in the range of mesopores. The higher specific surface area will increase the contact area of the electrode with electrolyte, and mesoporous nanostructure could shorten the lithium ions transport path. Both of these characteristics would enhance the electrochemical properties of the electrode.

The surface chemical composition and the oxidation states of the elements in NiFe$_2$O$_4$/N-C are analyzed using XPS and the corresponding spectra are shown in **Figure 4.** The survey spectrum (**Figure 4A**) indicates that the composite is composed of Ni, Fe, O, C, and N elements, and no any other elemental signals are detected. This result is consistent with our synthesis process, and further proves that the co-existence of Ni and Fe metals and the present of N. The Fe 2p XPS core line (**Figure 4B**) reveal two peaks whose binding energies are at 711.2 and 724.3 eV, respectively, due to the Fe $2p_{3/2}$ and Fe $2p_{1/2}$ with spin-orbital splitting energy of 13 eV. For the transition metallic elements, $2p_{3/2}$ emission is generally more intensive than $2p_{1/2}$ one, as it is due to that $2p_{3/2}$ spin has a degeneracy of four states, while $2p_{1/2}$ has only two. According to the binding energies, and the splitting energy between $2p_{3/2}$ and $2p_{1/2}$ emissions, the Fe ions are in Fe (III) state (Chen et al., 2019). In addition, the presence of satellite peak at 719.1 eV with binding energy about 8 eV higher than the $2p_{3/2}$ emission suggests that only Fe (III) ions exists in the NiFe$_2$O$_4$ compound. Similarly, the Ni $2p_{3/2}$ and Ni $2p_{1/2}$ lines (**Figure 4C**) locate at 855.4 and 874.3 eV, while the corresponding shake-up satellite peaks for Ni $2p_{3/2}$ and Ni $2p_{1/2}$ signals appear at 860.6 and 880.0 eV,

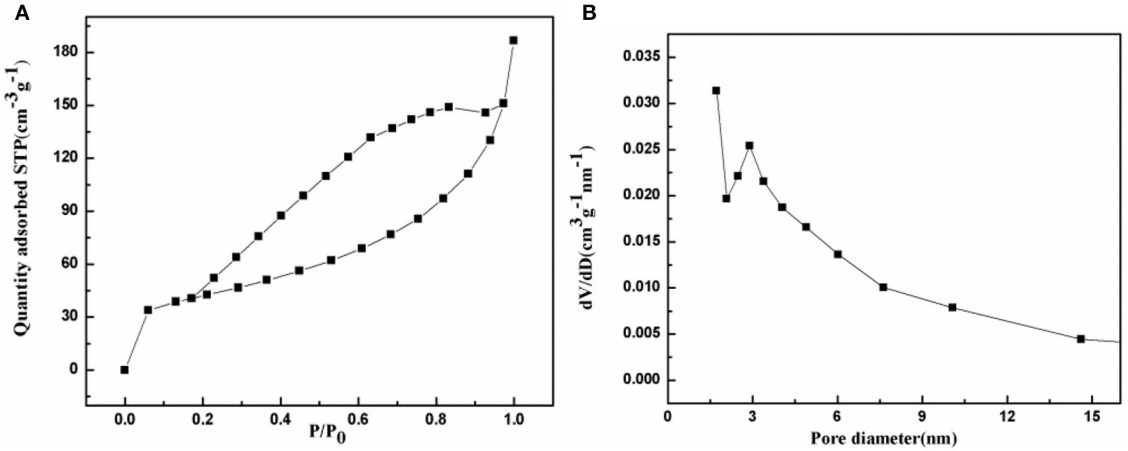

FIGURE 3 | (A) The N_2-sorption isotherms and **(B)** pore-size distribution of $NiFe_2O_4$/N-C.

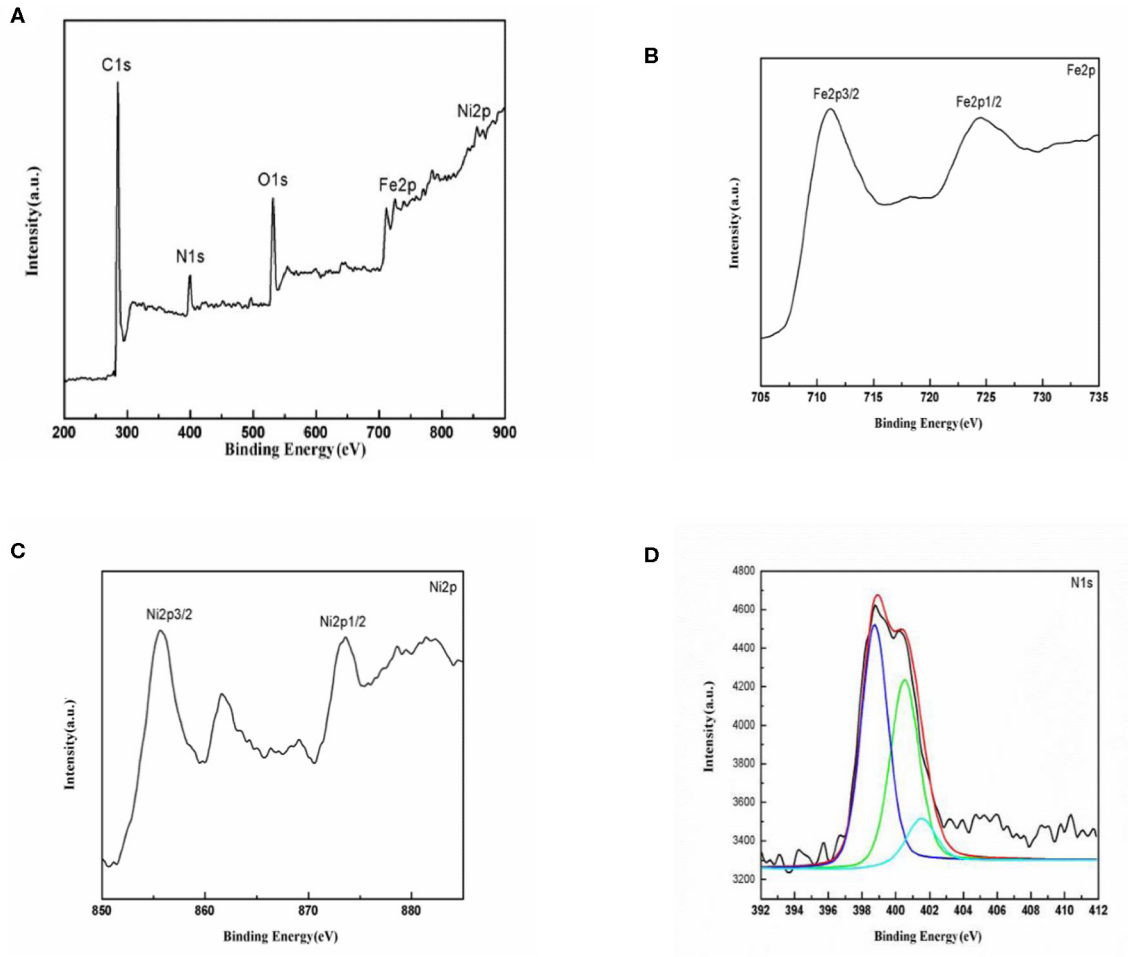

FIGURE 4 | XPS spectra of NiFe2O4/N-C composite. **(A)** Survey spectrum, **(B)** Fe 2p core level, **(C)** Ni 2p state, and **(D)** N 1s line.

respectively. These results imply that the Ni ions in $NiFe_2O_4$ are in +2 oxidation state (Zhao et al., 2018). The elemental ratio between Fe and Ni are calculated based on the intensity of Fe 2p and Ni 2p lines, which is around 2.02. The XPS data companied with XRD results indicate that the target $NiFe_2O_4$ has been successfully synthesized. The high-resolution N 1s XPS spectrum shown in **Figure 4D** could be deconvoluted into three components with binding energies at 398.3, 400.5 and 401.2 eV assigned to pyridinic N (C-N-H), pyrrolic N (C=N-C), and graphitic N [N- $(C)_3$] species, respectively (Yan et al., 2018). The appearance of graphitic-N implies that N atoms are successfully doped into the carbon crystalline structure. The N-doping will further increase the electronic conductivity, promote the capacity, and enhance the Li ions transport properties on/in carbon matrix, because the presence of N ions would alter the electronic structure of carbon matrix (Sun et al., 2016; Li et al., 2017).

The cyclic voltammetric (CV) curves of the $NiFe_2O_4$/N-C electrode for the initial four cycles are shown in **Figure 5A.** An intensive irreversible reduction peak at 0.35 V and a should peak at 0.12 V in the first cycle could be found and assigned to the reductions of Ni^{2+} to Ni and Fe^{3+} to Fe in $NiFe_2O_4$, the intercalation of Li ions into N-doped carbon matrix, and the formation of solid electrolyte interface (SEI) layers and Li oxides (Cherian et al., 2013; Ding et al., 2013). The chemical reaction formula of $NiFe_2O_4$ with Li is indicated as Equation (1), eight electrons should be transferred for one $NiFe_2O_4$ unit,

$$NiFe_2O_4 + 8Li \leftrightarrow Ni + 2Fe + 4Li_2O \quad (1)$$

A significant intensity decreasing is observed in the subsequent cycles and its cathodic potential shifts to the positive direction from 0.35 to 0.72 V. This is because that less SEI films will form in the second cycle compared with the first cycle. A small cathodic peak at 1.23 V is observed in first cycle and then moves to 1.25 V in following cycles. In the first anodic process, the multi-step oxidations of Ni and Fe to NiO and Fe_2O_3 result in the appearance of a broad oxidation peak at 1.67 V and a should peak at 1.81 V as well as the partial decomposition of

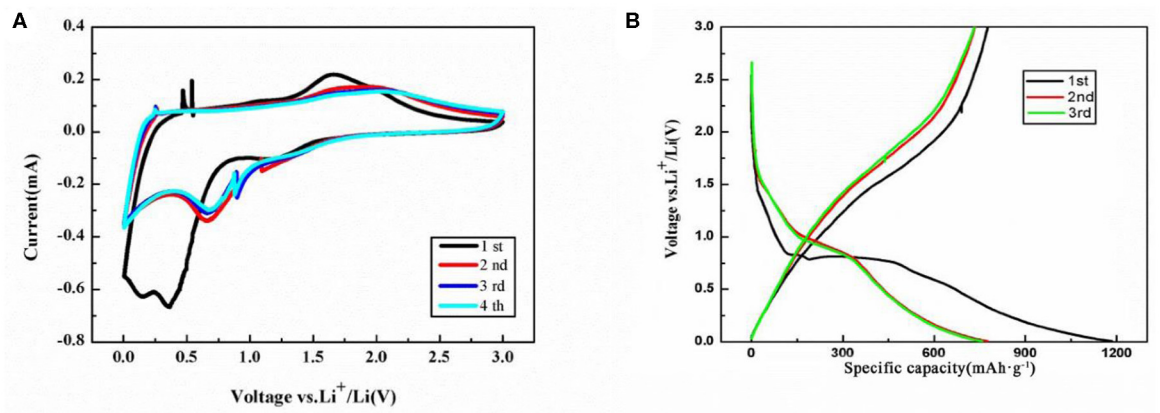

FIGURE 5 | (A) CV curve and **(B)** charge-discharge profiles of the NiFe2O4/N-C electrode. The scan rate is 0.2 mV/s, and potential range is 0.005–3.0 V.

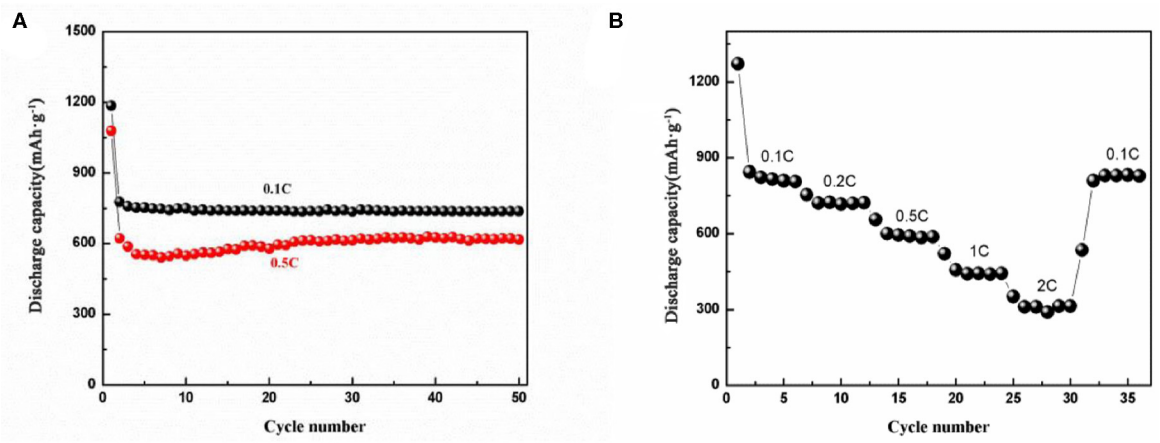

FIGURE 6 | (A) Cycling and **(B)** rate performances of NiFe2O4/N-C electrode (1C = 1,000 mA g^{-1}).

SEI films. In the subsequent cycles, the anodic peaks shift to around 1.75 and 2.00 V, which indicates that the electrochemical reversibility of the electrode gradually formed (Xia et al., 2012; Liu J. et al., 2017) and the reduction in polarization. The remarkably similar CV curves could be observed after the third cycle, suggesting the stable reversible reaction and good capacity retention.

Consistent with the CV data, similar current peaks can be identified in the voltage profiles for NiFe$_2$O$_4$/N-C electrode at the density of 0.1 C as shown in **Figure 5B.** It possesses a short flat following with a long flat. The initial discharges/charge capacities of the electrode are 1,193 and 773 mAh g^{-1} with the corresponding Coulombic efficiency of 64.8%. At the second cycle, the discharge/charge capacities are 771 and 749 mAh g^{-1}, whose Coulombic efficiency increases to 97.1%. After the second cycle, the potential-capacity profile is highly overlaid, indicating the good electrochemical reversibility.

Figure 6A shows the cycling performance of the electrode at 0.1 and 0.5 C (1 C = 1,000 mA g^{-1}) current densities. Both capacities decrease at the second cycle due to the irreversible formation of SEI layers in the first cycle. At 0.1 C, agreeing with the CV curves, the capacity at following cycles keeps constant. For 0.5 C, there is slight increase in capacity from 10 to 25 cycles, and then it maintains constantly. The capacity increasing may attribute to the activation of the NiFe$_2$O$_4$ embedded inside the carbon matrix. The capacities remain 760 and 610 mAh g^{-1} after 50 cycles at 0.1 and 0.5 C current densities, respectively. As shown in **Figure 6B,** the rate performance of the electrode appears a ladder-like reduction with increasing of the current density. At each current density, the specific capacity almost remains constant. It delivers a charge capacity of 815.2, 722.3, 602.3 mAh g^{-1} at 0.1 C, 0.2 C, and 0.5 C. When the current density increased to 1 C and even 2 C, the NiFe$_2$O$_4$/N-C electrode still delivers charge capacities of 442.2 and 311.3 mAh g^{-1}. When the rate decreases from 2 to 0.1 C, the capacity increases quickly to 830.3 mAh g^{-1}. Such a rate performance is superior than most of the single-metal oxide (Fe$_2$O$_3$ and NiO) (Feng et al., 2016; Pang et al., 2016; Wang et al., 2017b) and also is greater than other NiFe$_2$O$_4$ nanostructured electrodes e.g., NiFe$_2$O$_4$/CNTs and NiFe$_2$O$_4$ nanoparticles/MWCNTs (Mujahid et al., 2019; Zou et al., 2020). The main reasons for the excellent electrochemical properties include: (1) mesopores nanostructure provides various path way for lithium ion transportation and as a buffer to accommodate the volume change of electrode during charge/discharge process; (2) 3D nanorod framework shortens the migration path and enhances the Li ions diffusion coefficient and prevents aggregation of the CoFe$_2$O$_4$ nanoparticles, making them well-dispersed and effectively-utilized during repeated cycling (Weng et al., 2020); (3) the N-doping could enhance the electronic conductivity of carbon matrix, which would further enhance the electron and lithium ions transport inside the carbon matrix (Jia et al., 2020).

CONCLUSIONS

The NiFe$_2$O$_4$/N-doped carbon composite electrode exhibited good electrochemical characteristics, such as cycling stability showing reversible capacity of 760 mAh g^{-1} at 0.1 C upon 50 cycles, and excellent rate capability (442.2 mAh g^{-1} at 1 C). The main reasons for the excellent electrochemical properties are contributed to the mesoporous 3D nanostructure and N-doping in the carbon matrix. The MOFs-derived 3D carbon matrix nanostructure would effectively embed the NiFe$_2$O$_4$ nanocrystals inside the carbon matrix avoiding their aggregation. The mesoporous 3D structure could release the volume change during charge/discharge cycling maintaining the structure integrality. The good cycle performance confirms the advantages of bi-metallic oxides over single-metal ones as anode materials.

DATA AVAILABILITY STATEMENT

All datasets generated for this study are included in the article/**Supplementary Material**.

AUTHOR CONTRIBUTIONS

All authors listed have made a substantial, direct and intellectual contribution to the work, and approved it for publication.

FUNDING

This work was supported by Science and Technology Project of Fujian Province (No. 2018Y0064), Science and Technology Project of Xiamen City of China (No. 3502Z20173029), and Educational Scientific Research Project for Young and Middle-aged Teachers of Fujian Province (JA15261).

ACKNOWLEDGMENTS

The authors acknowledge Prof. Qi-Hui Wu for helpful discussion on this project.

SUPPLEMENTARY MATERIAL

The Supplementary Material for this article can be found online at: https://www.frontiersin.org/articles/10.3389/fmats.2020.00178/full#supplementary-material

REFERENCES

Bai, J., Li, X. G., Liu, G. Z., Qian, Y. T., and Xiong, S. L. (2014). Unusual formation of ZnCo$_2$O$_4$ 3D hierarchical twin microspheres as a high-rate and ultralong-life lithium-ion battery anode material. *Adv. Funt. Mater.* 24, 3012–3020. doi: 10.1002/adfm.201303442

Chen, Q., Sun, S., Zhai, T., Yang, M., Zhao, X., and Xia, H. (2018). Yolk–Shell NiS2 nanoparticle-embedded carbon fibers for flexible fiber-shaped sodium battery. *Adv. Energy Mater.* 8:1800054. doi: 10.1002/aenm.201800054

Chen, Q., Wang, R., Lu, F., Kuang, X., Tong, Y., and Lu, X. (2019). Boosting the oxygen evolution reaction activity of NiFe$_2$O$_4$ nanosheets by

phosphate ion functionalization. *ACS Omega* 4:3493. doi: 10.1021/acsomega.8b03081

Cherian, C. T., Sundaramurthy, J., Reddy, M. V., Suresh Kumar, P., Mani, K., and Pliszka, D. (2013). Morphologically robust NiFe2O4 nanofibers as high capacity Li-ion battery anode material. *ACS Appl. Mater. Interface* 5, 9957–9963. doi: 10.1021/am401779p

Ding, Y., Yang, Y., and Shao, H. (2013). One-pot synthesis of NiFe$_2$O$_4$/C composite as an anode material for lithium-ion batteries. *J. Power Sources* 244, 610–613. doi: 10.1016/j.jpowsour.2013.01.043

Feng, Y., Zhang, H., Li, W., Fang, L., and Wang, Y. (2016). Targeted synthesis of novel hierarchical sandwiched NiO/C arrays as high-efficiency lithium ion batteries anode. *J. Power Sources* 301, 78–86. doi: 10.1016/j.jpowsour.2015.09.101

Gao, X., Wang, J., and Zhang, D. (2017). Hollow NiFe$_2$O$_4$ nanospheres on carbon nanorods as a highly efficient anode material for lithium ion batteries. *J. Mater. Chem. A* 5, 5007–5012. doi: 10.1039/C6TA11058D

Hong, J. H., Jung, Y., and Kim, S. (2020). Synthesis of bi-metallic organic frameworks and their capacitive behaviors according to metal mixing ratio. *J. Nanosci. Nanotech.* 20, 2987–2991. doi: 10.1166/jnn.2020.17467

Jia, Q.-C., Zhang, H.-J., and Kong, L.-B. (2020). Nanostructure-modified *in-situ* synthesis of nitrogen-doped porous carbon microspheres (NPCM) loaded with FeTe$_2$ nanocrystals and NPCM as superior anodes to construct high-performance lithium-ion capacitors. *Electrochim. Acta* 337:135749. doi: 10.1016/j.electacta.2020.135749

Joshi, B., Samuel, E., Kim, M.-W., Kim, K., Kim, T.-G., Swihart, M. T., et al. (2019). Electrosprayed graphene films decorated with bimetallic (zine-iro)) oxide for lithium-ion battery anodes. *J. Alloys Compounds* 782, 699–708. doi: 10.1016/j.jallcom.2018.12.170

Li, J., Zhang, F., Wang, C., Shao, C., Li, B., Li, Y., et al. (2017). Self nitrogen-doped carbon nanotubes as anode materials for high capacity and cycling stability lithium-ion batteries. *Material Design* 133, 169–175. doi: 10.1016/j.matdes.2017.07.060

Lian, X., Cai, M., Qin, L., Cao, Y., and Wu, Q.-H. (2016). Synthesis of hierarchical nanospheres Fe$_2$O$_3$/graphene composite and its application in lithium-ion battery as a high-performance anode material. *Ionics* 22, 2015–2020. doi: 10.1007/s11581-016-1749-3

Liu, J., Xiao, J., Zeng, X., Dong, P., Zhao, J., Zhang, Y., et al. (2017). Combustion synthesized macroporous structure MFe$_2$O$_4$ (M= Zn, Co) as anode materials with excellent electrochemical performance for lithium ion batteries. *J. Alloys Compd*. 699, 401–407. doi: 10.1016/j.jallcom.2016.12.225

Liu, X., Zhang, T., Qu, Y., Tian, G., Yue, H., and Zhang, D. (2017). Carbonized polydopamine coated single-crystalline NiFe$_2$O$_4$ nanooctahedrons with enhanced electrochemical performance as anode materials in a lithium ion battery. *Electrochim. Acta* 231, 27–35. doi: 10.1016/j.electacta.2017.02.020

Luo, L., Cui, R., and Liu, K. (2015). Electrospun preparation and lithium storage properties of NiFe$_2$O$_4$ nanofibers. *Ionics* 21, 687–694. doi: 10.1007/s11581-014-1213-1

Luo, L., Yang, H., Bai, Z., Tao, D., Zhang, S., Xu, W., et al. (2017). Polyvinlpyrrolidone-derived carbon-coated magnesium ferrite composite nanofibers as anode material for high-performance lithium-ion batteries. *Ionics* 24, 297–301. doi: 10.1007/s11581-017-2317-1

Maiti, S., Pramanik, A., Dhawa, T., Sreemany, M., and Mahanty, S. (2018). Bi-metal organic framework derived nickel manganese oxide spinel for lithium-ion battery anode. *Mater. Sci. Eng. B* 229, 27–36. doi: 10.1016/j.mseb.2017.12.018

Mujahid, M., Ullah Khan, R., Mumtaz, M., Mubasher, Soomro, S. A., and Ullah, S. (2019). NiFe$_2$O$_4$ nanoparticles/MWCNTs nanohybrid as anode material for lithium-ion battery. *Ceram. Int.* 45 (7, Part A):8486-93. doi: 10.1016/j.ceramint.2019.01.160

Pang, H., Guan, B., Sun, W., and Wang, Y. (2016). Metal-organic-frameworks derivation of mesoporous NiO nanorod for high-performance lithium ion batteries. *Electrochim. Acta* 213, 351–357. doi: 10.1016/j.electacta.2016.06.163

Shao, C., Zhang, F., Li, B., Li, Y., Wu, Q.-H., and Yang, Y. (2017). Helical mesoporous carbon nanoribbons as high performance lithium ion battery anode materials. *J. Taiwan Inst. Chem. Eng.* 80, 434–438. doi: 10.1016/j.jtice.2017.07.036

Sun, B., Zhou, W., Li, H., Ren, L., Qiao, P., Li, W., et al. (2018). Synthesis of particulate hierarchical tandem heterojunctions toward optimized photocatalytic hydrogen production. *Adv. Mater.* 30:e1804282. doi: 10.1002/adma.201804282

Sun, H., Wang, Q., Geng, H., Li, B., Li, Y., Wu, Q.-H., et al. (2016). Fabrication of chiral mesoporous carbonaceous nanofibers and their electrochemical energy storage. *Electrochim. Acta* 213, 752–760. doi: 10.1016/j.electacta.2016.08.005

Wang, C., Li, Y., Ruan, Y., Jiang, J., and Wu, Q.-H. (2017a). ZnFe$_2$O$_4$-nanocrystal-assembled microcages as an anode material for high performance lithium-ion batteries. *Mater. Today Energy* 3, 1–8. doi: 10.1016/j.mtener.2016.12.001

Wang, C., Zhang, Y., Li, Y., Liu, J., Wu, Q.-H., Jiang, J., et al. (2017b). Synthesis of fluorine-doped α-Fe2O3 nanorods toward enhanced lithium storage capacity. *Nanotechnology* 28:065401. doi: 10.1088/1361-6528/aa53b3

Wang, J., Yang, G., Wang, L., and Yan, W. (2016). Synthesis of one-dimensional NiFe$_2$O$_4$ nanostructures: tunable morphology and high-performance anode materials for Li ion batteries. *J. Mater. Chem. A* 4, 8620–8629. doi: 10.1039/C6TA02655A

Wang, N., Xu, H. Y., Chen, L., Gu, X., Yang, J., and Qian, Y. T. (2014). A general approach for MFe$_2$O$_4$ (M = Zn, Co, Ni) nanorods and their high performance as anode materials for lithium ion batteries. *J. Mater. Chem. A* 247, 163–169. doi: 10.1016/j.jpowsour.2013.08.109

Wang, Y., Zhu, X., Liu, D., Tang, H., Luo, G., Tu, K., et al. (2018). Synthesis of MOF-74-derived carbon/ZnCo$_2$O$_4$ nanoparticles@CNT-nest hybrid materials and its application in lithium ion batteries. *J. Appl. Electrochem.* 49, 1103–1112. doi: 10.1007/s10800-019-01349-4

Weng, S., Huo, T., Liu, K., Zhang, J., and Li, W. (2020). *In-situ* polymerization of hydroquinone-formaldehyde resin to construct 3D porous composite LiFePO4/carbon for remarkable performance of lithium-ion batteries. *J. Alloy Compd.* 818:152858. doi: 10.1016/j.jallcom.2019.152858

Wu, K., Liu, D., and Tang, Y. (2018). *In-situ* single-step chemical synthesis of graphene-decorated CoFe$_2$O$_4$ composite with enhanced Li ion storage behaviors. *Electrochim. Acta* 263, 515–523. doi: 10.1016/j.electacta.2018.01.047

Wu, Q.-H., Qu, B., Tang, J., Wang, C., Wang, D., Li, Y., et al. (2015). An alumina-coated Fe$_3$O$_4$-reduced graphene oxide composite electrode as a stable anode for lithium-ion battery. *Electrochim. Acta* 156, 147–153. doi: 10.1016/j.electacta.2014.12.149

Xia, H., Zhu, D., Fu, Y., and Wang, X. (2012). CoFe$_2$O$_4$-graphene nanocomposite as a high-capacity anode material for lithium-ion batteries. *Electrochim. Acta* 83, 166–174. doi: 10.1016/j.electacta.2012.08.027

Xiao, Y., Zai, J., Tian, B., and Qian, X. (2017). Formation of NiFe$_2$O$_4$/expanded graphite nanocomposites with superior lithium storage properties. *Nano-Micro Lett.* 9:34. doi: 10.1007/s40820-017-0127-7

Xing, Z., Ju, Z., Yang, J., Xu, H., and Qian, Y. (2013). One-step solid state reaction to selectively fabricate cubic and tetragonal CuFe$_2$O$_4$ anode material for high power lithium ion batteries. *Electrochim. Acta* 102, 51–57. doi: 10.1016/j.electacta.2013.03.174

Xiong, Q., Tu, J., Shi, S., Liu, X., Wang, X., and Gu, C. (2014). Ascorbic acid-assisted synthesis of cobalt ferrite (CoFe$_2$O$_4$) hierarchical flower-like microspheres with enhanced lithium storage properties. *J. Power Sources* 256, 153–159. doi: 10.1016/j.jpowsour.2014.01.038

Yan, X.-L., Li, H.-F., Wang, C., Jiang, B.-B., Hu, H.-Y., Xie, N., et al. (2018). Melamine as a single source for fabrication of mesoscopic 3D composites of N-doped carbon nanotubes on graphene. *RSC Adv.* 8, 12157–12164. doi: 10.1039/C8RA01577E

Yang, H., Zhang, K., Wang, Y., Yan, C., and Lin, S. (2018). CoFe$_2$O$_4$ derived-from bi-metal organic frameworks wrapped with graphene nanosheets as advanced anode for high-performance lithium ion batteries. *J. Phys. Chem. Solids* 115, 317–321. doi: 10.1016/j.jpcs.2017.12.042

Yang, S., Han, Z., Zheng, F., Sun, J., Qiao, Z., Yang, X., et al. (2018). ZnFe$_2$O$_4$ nanoparticles-cotton derived hierarchical porous active carbon fibers for high rate-capability supercapacitor electrodes. *Carbon* 134, 15–21. doi: 10.1016/j.carbon.2018.03.071

Zhai, T., Sun, S., Liu, X., Liang, C., Wang, G., and Xia, H. (2018). Achieving insertion-like capacity at ultrahigh rate via tunable surface pseudocapacitance. *Adv. Mater.* 30:1706640. doi: 10.1002/adma.201706640

Zhao, J., Li, X., Cui, G., and Sun, X. (2018). Highly-active oxygen evolution electrocatalyzed by an Fe-doped $NiCr_2O_4$ nanoparticle film. *Chem. Commun.* 54, 5462–5465. doi: 10.1039/C8CC02568A

Zhou, F., Hu, X., and Li, Z. (2014). MOF-derived porous $ZnO/ZnFe_2O_4$/C octahedra with hollow interiors for high-rate lithium-ion batteries. *Adv. Mater.* 26, 6622–6628. doi: 10.1002/adma.201402322

Zou, Y., Li, Z., Liu, Y., Duan, J., and Long, B. (2020). Coaxial structure of $NiFe_2O_4$/CNTs composites as anodes for enhanced lithium ion batteries. *J. Alloy Compd.* 820:153085. doi: 10.1016/j.jallcom.2019.153085

Conflict of Interest: The authors declare that the research was conducted in the absence of any commercial or financial relationships that could be construed as a potential conflict of interest.